Published in final edited form as:
Biomaterials. 2013 January ; 34(2): . doi:10.1016/j.biomaterials.2012.09.055.

The use of native chemical functional groups presented by wound beds for the covalent attachment of polymeric microcarriers of bioactive factors

Rishabh Jain[a], **Ankit Agarwal**[a], **Patricia R. Kierski**[b], **Michael J. Schurr**[c], **Christopher J. Murphy**[d,***], **Jonathan F. McAnulty**[b,**], and **Nicholas L. Abbott**[a,*]

[a]Department of Chemical and Biological Engineering, University of Wisconsin-Madison

[b]Department of Surgery, School of Veterinary Medicine, University of Wisconsin-Madison

[c]Department of Surgery, School of Medicine and Public Health, University of Colorado-Denver

[d]Department of Ophthalmology & Vision Science, School of Medicine and the Department of Surgical and Radiological Sciences, School of Veterinary Medicine, University of California-Davis

Abstract

The development of versatile methods that provide spatial and temporal control over the presentation of physical and biochemical cues on wound beds can lead to new therapeutic approaches that expedite wound healing by favorably influencing cellular behaviors. Towards that goal, we report that native chemical functional groups presented by wound beds can be utilized for direct covalent attachment of polymeric microbeads. Specifically, we demonstrated the covalent attachment of maleimide-functionalized and catechol-functionalized microbeads, made of either polystyrene (non-degradable) or poly(lactic-co-glycolic acid) ((PLGA), degradable), to sulfhydryl and amine groups present on porcine dermis used here as an *ex vivo* model wound bed. A pronounced increase (10–70 fold) in the density and persistence of the covalently reactive microbeads was observed relative to microbeads that adsorb via non-covalent interactions. Complementary characterization of the surface chemistry of the *ex vivo* wound beds using Raman microspectroscopy provides support for our conclusion that the increased adherence of the maleimide-functionalized beads results from their covalent bond formation with sulfhydryl groups on the wound bed. The attachment of maleimide-functionalized microbeads to wounds created in live wild-type and diabetic mice led to observations of differential immobilization of microbeads on them and were consistent with anticipated differences in the presentation of sulfhydryl groups on the two different wound types. Finally, the incorporation of maleimide-functionalized microbeads in wounds created in wild-type mice did not impair the rate of wound closure relative to an untreated wound. Overall, the results presented in this paper enable a general and facile approach to the engineering of wound beds in which microbeads are covalently immobilized to wound beds. Such immobilized microbeads could be used in future studies to release bioactive factors (e.g., antimicrobial agents or growth factors) and/or introduce topographical cues that promote cell behaviors underlying healing and wound closure.

[*]Corresponding authors: Prof. N. L. Abbott, Department of Chemical and Biological Engineering, University of Wisconsin, 1415 Engineering Drive, Madison, WI 53706 (USA), abbott@engr.wisc.edu. [**]Prof. J.F. McAnulty, Department of Surgical Sciences, School of Veterinary Medicine, University of Wisconsin, 2015 Linden Drive, Madison, WI 53706., mcanultj@svm.vetmed.wisc.edu. [***]Prof. C.J. Murphy, School of Veterinary Medicine, Department of Surgical and Radiological Sciences, 1423 Tupper Hall, University of California, Davis, CA 95616-8745, USA., cjmurphy@ucdavis.edu.

Keywords

Wound healing; Wound bed engineering; Microspheres; Dopamine; Catechols; Maleimide; Diabetic wounds; Raman spectroscopy

INTRODUCTION

Conventional wound dressings promote healing by acting primarily as 'barriers' that prevent the entry of microbes and regulate the exit of blood, nutrients and water from wounds. When conventional dressings are used, wound closure occurs predominantly as the result of the endogenous healing capacity of the wound [1]. In contrast, a range of new approaches to wound healing are being explored based on the delivery of 'bioactive' agents such as (1) antimicrobial agents that prevent infection and (2) exogenous growth factors that can act as biochemical cues to promote wound healing via accelerated re-epithelialization, angiogenesis and granulation tissue formation [2]. In addition, a number of recent *in vitro* studies have shown that cell behaviors that underlie wound healing can also be promoted by nanotopographical [3–5] and micromechanical [6–8] cues. In summary, it is becoming increasingly apparent that the appropriate integration of biochemical, nanotopographical and micromechanical cues that trigger favorable cell behaviors in wounds has the potential to form the basis of a general and facile approach that enables faster wound healing.

The concept of delivering biochemical factors to wounds with the goal of accelerating wound healing is not new. For example, exogenous delivery of growth factors by topical application has been explored. However, these approaches have generally found to be ineffective [9–11] as the soluble growth factors delivered to the wound in these approaches were either proteolysed [12], sequestered by secreted macromolecules (e.g. fibrinogen, α-2-macroglobulin) [13], or removed by exudate before reaching the wound bed. In addition, delivery of antimicrobial agents from conventional dressings has also been investigated [14, 15]. Approaches explored to date, however, lead to the delivery of large and uncontrolled amounts of the antimicrobial agents to wounds and surrounding areas, resulting in tissue toxicity and impaired wound healing [16, 17]. Thus, in order to realize the potential benefits of bioactive factors for accelerated wound healing, it is evident that improved approaches are needed to deliver controlled quantities of bioactive agents to wound beds. The study reported in this paper was motivated by the hypothesis that the presentation of bioactive factors on wound beds in a spatially and temporally controlled manner has the potential to improve the efficacy of wound healing approaches based on use of such bioactive factors. To enable the testing of this hypothesis, herein we report an investigation that sought to determine if a wound bed presents native chemical functional groups that can be exploited for the covalent attachment (and thus controlled and prolonged adherence) of polymeric carriers (macromolecules or microbeads) capable of delivering physical cues and bioactive factors.

As described below, we investigated the covalent attachment of degradable and non-degradable beads to the surfaces of model wound beds. The focus on degradable microbeads is motivated by the observation that microbeads are promising delivery vehicles for protein-based therapeutics in harsh wound microenvironments because they protect their encapsulated contents from proteolysis or exudate removal. In addition, a number of past studies have demonstrated that microbeads can enable sustained delivery of bioactive agents via slow degradation [18]. For example, slowly degrading microbeads that encapsulate bioactive factors have been fused to create synthetic scaffolds [19, 20] or mixed within hydrogels [21, 22] to enable the sustained delivery of bioactive factors in tissue engineering applications. We also investigated non-degradable beads because covalent immobilization of

non-degradable microbeads on wound beds may provide the basis of methods to modify the nanotopography and mechanical stiffness of wound beds *in vivo*, which can also promote favorable cell behaviors [4, 5, 23] that ultimately accelerate wound healing. For example, in one study, four different human vascular endothelial cell-types were found to exhibit favorable alignment and increased migration rates along topographic ridges with sizes between 800–1200 nm [4]. Past studies have also established that the differentiation of fibroblasts to myofibroblasts (which promote tissue repair by secreting collagen and contracting the ECM) is dependent on substrate stiffness and occurs at a stiffness upwards of 20 kPa [6]. In this article, we show that microbeads (with diameters of 500 nm or 1000 nm) can be attached covalently to specific chemical groups (amine and sulfhydryl) present on wound beds and that covalently bound microbeads have a substantially higher persistence relative to physically adsorbed microbeads.

During the process of wound healing, precursor peptides (such as procollagen [24], tropoelastin, and fibrillin [25]) of various structural proteins (such as collagen and elastin), and other cell-adhesion proteins (such as fibronectin [26] and laminin [27]) that are rich in cysteines (which contain free sulfhydryl groups) and lysines (which contain free amine groups) are secreted extracellularly. These peptides and proteins help form either the fibrin clot (fibrinogen), granulation tissue (collagen type-III) or the redeposited extracellular matrix (collagen type-I, elastin). The lysines and cysteines in collagen/elastin are not present at comparable levels in normal/healed skin tissue because they are enzymatically modified to form cross-links (hydroxylysyl or disulfide linkages) [28, 29] in their mature protein forms. Fibronectin also diminishes to lower levels in healed tissue. The focus of our study was motivated additionally by the hypothesis that differing quantities of secreted precursor peptides across a wound surface may lead to the presentation of heterogeneous spatial distributions of amine and sulfhydryl moieties. Such spatial variation in the presentation of functional groups may lead to patterned immoblization of microbeads via covalent attachment. Indeed, as reported below, the experiments reported in this paper indicate spatial variation in the availability of reactive, chemical moeities on model wound beds. Here we note that past studies performed *in vitro* have suggested that heterogeneity in the density of immobilized growth factors can accelerate fundamental cell behaviors such as cell migration and proliferation [30, 31]. Another key merit of covalently attaching microbeads to wound beds is that it enables rational control of the density of microbeads that are attached to the wound bed. Below, we illustrate this potential using two different approaches: (i) by varying the time over which amine-reactive microbeads are reacted with model wound beds, or (ii) by introducing a pre-treatment step that involves the chemical reduction of disulfide linkages on wound beds to free sulfhydryl groups to which microbeads are attached covalently.

In the present study, porcine dermis was used as an *ex vivo* model of a partial-thickness wound. As the structural components of porcine skin, such as the epidermis, dermis and subdermal structures, are considered similar to human skin [34], porcine dermis is generally viewed as an appropriate *ex vivo* model for partial-thickness wounds in humans. Well established models of excised dermal wounds in either normal wild-type or diabetic (db/db) mice were used as model *in vivo* full-thickness wound beds [32, 33] in our study.

MATERIALS AND METHODS

2.1 Materials

1-Ethyl-3-(3-dimethylaminopropyl)carbodiimide hydrochloride (EDC) and sulfosuccinimidyl-4-(N-maleimidomethyl)cyclohexane-1-carboxylate (Sulfo-SMCC) were purchased from Thermo Fisher Scientific (Rockford, IL). Dopamine-HCl, tris(hydroxymethyl)aminomethane hydrochloride (Tris-HCl), 2-mercaptoethanol (BME),

reduced L-glutathione (GSH) and 4-morpholineethanesulfonic acid monohydrate (MES) were purchased from Sigma-Aldrich (St. Louis, MO). Amine-coated and carboxylate-coated fluorescent (yellow-green, excitation/emission - 505/515 nm) microbeads made from polystyrene were purchased from Invitrogen (Carlsbad, CA). Amine-coated and carboxylate-coated fluorescent (yellow-green, excitation/emission - 505/515 nm) microbeads, made from 50:50 Poly(lactic-co-glycolic acid) (PLGA) of molecular weight range 30–60 kDa (Inherent Viscosity: 0.55–0.75), were purchased from Phosphorex (Fall River, MA). Deionized water (resistivity: 18.2 MΩ-cm) was used in all the experiments wherever required. Dulbecco's phosphate buffered saline (PBS, pH 7.4) was purchased from Mediatech (Manassas, VA). 24-well plates were purchased from BD Biosciences (Bedford, MA).

2.2 Synthesis of maleimide-functionalized microbeads

Amine-coated, fluorescent microbeads made from PLGA (diameter: 0.5 μm) or polystyrene (diameter: 1 μm) were functionalized with sulfhydryl reactive maleimide groups on their surface by reaction with the heterobifunctional cross-linker sulfo-SMCC which contains both maleimide and sulfo-succinimidyl (amine reactive) groups.

Aliquots of 12.5 mg/mL (~5.75×10^9 microbeads/mg) of the lyophilized PLGA microbeads or 100 μL of the polystyrene microbead suspension (~3×10^{10} microbeads/mL) were functionalized using the procedures described below. The microbeads were rinsed to remove cryoprotectants, surfactants and/or other stabilizers present in the purchased materials. This was done by their suspension in PBS (300 μL; pH 7.4) followed by centrifugation (8,000 rpm, 5 min) and removal of supernatant for a total of three times. The microbeads were then resuspended in PBS (150 μL; pH 7.4) and mixed with sulfo-SMCC solution (150 uL; 10 mg/mL in PBS, pH 7.4) and the reaction was allowed to proceed for 30 min. Thereafter, the microbeads were rinsed by centrifugation (8,000 rpm, 5 min), removal of supernatant and suspension in PBS (300 μL; pH 7.4) three times. The polystyrene microbeads were resuspended in PBS (pH 7.4, 10 mL, final concentration: ~3×10^9 microbeads/ml) just before their use. The final concentration of PLGA microbeads in PBS was such that the specific surface area/mL of microbeads was the same as that of the polystyrene beads.

Maleimide-functionalized microbeads (200 μL, 1% w/w) whose reactivity was quenched were prepared by the addition of β-mercaptoethanol (99%, 10 μL) to the microbead suspension and incubation overnight. Subsequently, the quenched microbeads were rinsed with DI water thrice by centrifugation (8000 rpm, 5 min) and removal of supernatant and resuspended in PBS (pH 7.4), before use.

2.3 Synthesis of catechol-functionalized microbeads

Carboxylate-coated fluorescent microbeads made from either PLGA (lyophilized, diameter: 0.5 μm) or polystyrene (2% w/w solution, diameter: 1 μm) were functionalized with catechol groups by reacting the carboxylate groups with the amine group of dopamine using the cross-linker EDC. Briefly, either 100 μL of 12.5 mg/mL (~ 5.75×10^9 microbeads/mg) of the lyophilized PLGA microbeads or 100 μL of the stock polystyrene microbead suspension (~ 3×10^{10} microbeads/ml) were taken in an aliquot and then rinsed to remove cryoprotectants, surfactants and/or other stabilizers. This was done by their suspension in MES buffer solution (0.25 M, pH 5, 300 μL) followed by centrifugation (8,000 rpm, 5 min) and removal of supernatant three times. The microbeads were then resuspended in MES buffer solution (0.25 M, pH 5, 200 μL) and a freshly-prepared solution (200 μL) of dopamine (40 mg/mL) and EDC (20 mg/mL) buffered by MES (0.25 M, pH 5) was added. The reaction was allowed to proceed for 2 h. Subsequently, the microbeads were rinsed by centrifugation (8,000 rpm, 5 min) and suspension in MES buffer solution (0.25M, pH 5, 300 μL) three

times. The polystyrene microbeads were finally suspended in PBS (pH 7.4, 10 mL, final concentration: ~3×10^9 microbeads/mL) just before use. The final concentration of PLGA microbeads in PBS (pH 7.4) was adjusted such that the specific surface area of microbeads was the same as that of the polystyrene beads.

Catechol-functionalized microbeads (200 μL, 1% w/w) whose reactivity was quenched were prepared by the addition of β-mercaptoethanol (99%, 10 μL) and tris-HCl (5 mg) to the microbead suspension and incubation overnight. Subsequently, the quenched microbeads were rinsed with DI water thrice by centrifugation (8000 rpm, 5 min) and removal of supernatant, and resuspended in PBS (pH 7.4) before use.

2.4 ζ-potential Measurements

ζ-potential measurements were performed at room temperature with a Malvern Zetasizer 3000HS (Malvern Instruments Ltd., Worcestershire, UK). The concentration of the microbeads in suspension was 0.001 wt%. PBS buffer (1 mM, pH 7.4) or MES buffer (1 mM, pH 5) were used as suspension mediums. The zeta potential was determined at least five times for each sample.

2.5 Covalent attachment of microbeads to porcine dermis

Porcine dermis tissue was harvested using a Zimmer® dermatome from a Yucatan miniature pig (4–12 months old) that had been euthanized. The samples were 30/1000 inch thick and harvested from the shaved and scrubbed dorsum (back) of the pig and then frozen. Before use, samples were thawed at room temperature and cut into pieces (approx. size: 1×1 cm). The dermal side was used as a model wound bed (henceforward referred to as porcine dermis) for our experiments. Porcine dermis samples were incubated in 24-well plates and 1 ml. of reactive, quenched (control) or non-reactive (control) microbead suspension was added to each well. 5–6 replicates were used for each experimental sample. The samples were incubated with the microbeads for 30–90 minutes depending on the experiment. Thereafter, the samples were rinsed with a stream of deionized water and incubated with 1 ml. of PBS (pH 7.4) in wells of 24-well plates. The plates were placed overnight on a flat laboratory rotator operating at 40 rpm. Thereafter, the samples were rinsed again with a stream of deionized water and the samples were blotted with lint-free tissue before imaging.

2.6 Fluorescence microscopy, image processing and quantification of microbead attachment

All samples were imaged as 8-bit grayscale images using an inverted fluorescent microscope (Olympus IXZ1) with the appropriate filter set (Chroma 41004) and a 4× objective lens (N.A. 0.13). Four images from different regions of the sample were taken for every sample. In some cases, when the microbeads were located in multiple focal planes (due to wrinkling or topographical inhomogeneity in the sample), images from multiple focal planes were combined to get a composite image.

Images were processed using ImageJ (NIH, Bethesda, MD) to quantify the increment in fluorescence due to the attached microbeads on samples. Briefly, the images were sharpened and then a grayscale cutoff was applied consistently across all images to enable quantification of the fluorescent area of each sample due to the microbeads (see Figure S2). The percent area fraction of the sample covered by fluorescent microbeads was calculated as:

$$\frac{\text{Quantified fluorescent area}}{\text{Total image area}} \times 100$$

The number of microbeads immobilized per unit area (mm^2) was calculated as:

$$\frac{\text{Quantified fluorescent area (in } \mu m^2)}{K_{PF} \times \text{Image area (in } mm^2) \times A \text{ (in } \mu m^2)}$$

where A is the cross-sectional area of one microbead and K_{PF} is a prefactor that characterizes the optical cross-sectional area of the microbeads (relative to A) due to their fluorescent glow. The factor K_{PF} was determined by calibration experiments in which known quantities of microbeads were incubated on porcine dermis samples and then imaged. Based on these experiments, K_{PF} - was determined to be approximately 10 for both types of microbeads (PLGA and polystyrene).

2.7 Raman Spectroscopy

A confocal Raman microscope (LabRAM Aramis Horiba Jobin Yvon) with a 50X long-working distance (LWD) objective (N.A. 0.55) and a laser wavelength of 785 nm (10–20 mW of power at sampling point) was used to collect spectra. The confocal hole was opened to 200 μm to find the best compromise between axial resolution and signal intensity. The depth of focus is estimated at 1–10 μm. Spectra from three different points on each sample were measured and averaged. 2–3 replicates per sample were obtained. The total collection time for each spectrum was 5 min. The raw spectra were processed to remove background fluorescence and normalized using a MATLAB-based Raman processing program [35].

Spectra were also acquired from untreated and chemically treated (Refer Table 1) porcine dermis samples. After chemical treatment for 60 minutes, the samples were rinsed with a stream of deionized water, incubated in a salt wash solution (PBS, pH 7.4) overnight and rinsed again with a stream of deionized water.

2.8 Covalent immobilization of fluorescent, reactive microbeads on live mice wounds in vivo

All experimental protocols were approved by the Institutional Animal Care and Use Committee (IACUC) of the University of Wisconsin-Madison. Phenotypically normal male mice (wild-type for *Lepr^{db}*, Jackson Laboratories, Inc.) between the ages of 8–12 weeks were used. Mice were housed and fed as described elsewhere [36]. ‘Full-thickness’ dermal wounds were created on the flanks of mice anaesthetized with inhaled isoflurane, as described elsewhere [36]. A 6-mm biopsy punch was used to create ‘full-thickness’ dermal wounds of the flanks of the mice (8 mice per group; 2 wounds per mice). The wounds were incubated against a suspension containing either fluorescent PLGA maleimide-functionalized microbeads (covalently reactive to sulfhydryl groups) or amine-coated microbeads (non-reactive to sulfhydryl groups) (diameter: 0.5 μm; reactive and non-reactive control; 100 μL per wound; final concentration: ~7×10^9 microbeads/mL) for 30 mins. After the incubation with microbeads, the wounds were thoroughly rinsed 3 times with 0.5 mL PBS (pH 7.4). After incubation with microbeads, the mice were euthanized by intra-peritoneal injection of Beuthanasia®-D (Schering-Plough) solution (0.5 ml/mouse) and the wounds were harvested. Similar experiments were performed in the excisional wounds in diabetic mice (db/db mice, Jackson Laboratories, Inc.). The harvested wounds were imaged for fluorescent microbeads using a fluorescence microscope (Olympus IX70) equipped with the required fluorescence filter cubes (Chroma Technologies, Rockingham, VT).

2.9 Study of impairment of wound healing by reactive microbeads in wild-type mice

‘Full-thickness’ dermal wounds, 6 mm in diameter, were surgically created on the flanks of wild-type mice as described above (30 mice; 10 mice per group; 2 wounds per mice).

Silicone O-rings (McMaster-Carr®, inner diameter 11 mm, outer diameter 15 mm) were applied to the wounds to create a 'splinted' wound model, as described elsewhere [34]. Wounds were left uncovered and the mice were placed on a warming pad during recovery from anesthesia. Mice were monitored daily for signs of pain and illness, and weighed on days 0, 1, and 3 post-operatively, and every three days thereafter. At the end of the study, mice were euthanized by injection of Beuthanasia®-D (Schering-Plough) solution (0.5 ml/mouse) intra-peritoneally after induction of anesthesia as described above. For the duration of the studies, the splints and sutures were monitored daily. Any loss of contact between the splint and skin was repaired with tissue glue. Broken or missing sutures were replaced under anesthesia as described above, and a dose of buprenorphine was administered subcutaneously (0.1 mg/kg) for pain control. Wounds were removed from analysis if two or more sutures were broken or missing within a 24-hour period.

Mice were randomly assigned to either the control(s) or the experimental group on the day of surgery (10 wild-type mice per group, total n = 30 mice). The two control groups were (1) mice treated with the non-reactive amine-coated microbeads suspended in PBS and (2) mice treated with PBS (containing no microbeads). The wounds were incubated with 100 μL of a suspension of microbeads (diameter: 0.5 μm; reactive and non-reactive control; concentration: ~7×10^9 microbeads/mL) for 30 mins. After the incubation with microbeads, wounds were thoroughly rinsed 3 times with 0.5 mL PBS (pH 7.4) by pipetting repeatedly. Wounds were photographed on days 0, 1, and 3 post-operatively, and every two to three days thereafter. Wounds were traced and the area calculated in mm^2 using ImageJ (NIH, Bethesda, MD). Wound closure was calculated at each time point as the percentage of the original wound area.

2.10 Statistical analyses

The error bars in the graphs in this paper correspond to 2 times the Standard Error of Mean (2 × SEM) across replicates, unless otherwise mentioned. Significant difference between two groups was evaluated by Student's t-test assuming unequal variance and between more than two groups by one-way analysis of variance (ANOVA). The level of significance was set at $\alpha < 0.05$.

3. RESULTS AND DISCUSSION

3.1 Covalent attachment of catechol-functionalized microbeads to porcine dermis

The first class of reactive microbeads that we describe in this paper were surface functionalized with the catechol moeity. Several recent studies have demonstrated catechols to be reactive towards a wide variety of inorganic and organic surfaces, including noble metals, oxides, polymers, semiconductors and ceramics [37, 38]. They are also ubiquitously present in "natural glues" secreted by mussel byssus [39], bacterial biofilms [40] and fruit skin [41]. These past reports, when combined, indicate that catechols possess at least three attributes that make them promising candidates for covalent attachment of microbeads to wound beds, as investigated below. Firstly, catechols form addition products with both amine and sulfhydryl groups [42], both of which are found in tissue proteins. Secondly, catechols are stable and unreactive in acidic media and can be "switched on" to be reactive at physiological pH (slightly alkaline) [37]. In brief, and with reference to Figure 2A **(inset)**, when the catechol – *o*-quinone equilibrium shifts towards the right in response to the change in pH, the *o*-quinones irreversibly react with amine and sulfhydryl groups by Michael addition type reactions or Schiff-base coupling [43]. This characteristic allowed us to functionalize the microbeads at acidic pH (pH 5.0) and activate them by exposure to physiological pH (pH 7.4) at the time of their use. Thirdly, catechols react with surfaces

over a time period of 1–3 hours, which is sufficiently fast to allow for the potential translation of these procedures to clinical wound management.

We prepared catechol-functionalized microbeads (henceforth referred to as **CAT-microbeads**) from carboxylate-coated microbeads **(COOH-microbeads)**, as depicted in Figure 1A. Briefly, the carboxylic acid groups of COOH-microbeads were coupled to the amine groups of dopamine using EDC to mediate amide bond formation at pH 5.5. We measured the negative surface charge density of the COOH-microbeads (ζ-potential: −41.5±2.1 mV) to decrease in magnitude after transformation to CAT-microbeads (ζ-potential: −21.4±0.6 mV), a result that is consistent with replacement of carboxylic acid groups on the surface of microbeads by catechol groups (neutrally charged). As an additional control, we also prepared CAT-microbeads whose reactivity was quenched towards amine and sulfhydryl groups. This was achieved by reacting the CAT-microbeads with Tris (tris(hydroxymethyl) aminomethane (containing amine groups)) and β-mercaptoethanol (BME, containing sulfhydryl groups) overnight. The quenched CAT-microbeads were determined to have roughly the same surface charge density (ζ-potential: −22±0.8 mV) as CAT-microbeads.

The first experiment that we performed using the CAT-microbeads was designed to determine if they would exhibit stronger adherence to a wound-bed (higher density of microbeads over time) relative to the quenched CAT-microbeads and their precursor COOH-microbeads. These experiments were conducted using non-degradable beads made of polystyrene **(PS)** (diameter: 1 μm). As illustrated in Figure 2A, suspensions of CAT-microbeads were incubated on the harvested porcine dermis samples. We adjusted the pH of the microbead suspension from acidic (pH 5.0) to alkaline (pH 7.4) to activate the catechols for covalent reaction with the porcine dermis. After incubation of beads on the porcine dermis for a desired time period (30–90 min), the samples were placed overnight in PBS to simulate the general effect of wound exudate on the persistence of the microbeads on the model wound beds. We oberved that PBS caused the detachment of COOH-microbeads from the wound-bed, likely due to the screening of ionic interactions of the carboxylic groups of COOH-microbeads with the tissue surface. Fluorescence imaging of porcine dermis samples following the treatments described above (see fluorescent images in Figure 3A–F) hint that a higher density of CAT-microbeads (PS) remained attached to porcine dermis samples relative to COOH-microbeads (PS) or quenched CAT-microbeads (PS) after overnight incubation in PBS (see Figure 3G and 3H for statistically significant quantitation of the densities of beads on the surfaces). Although inspection of Figures 3A–F reveals the presence of some aggregates of microbeads on the model wound, a quantitative analysis of the images (Figure S3) reveals that most of the fluorescence is due to a cluster of 1–4 microbeads. We also note that without the overnight incubation in PBS, the attached microbeads densities were similar for both CAT- microbeads and the controls (data not shown). Overall, these results are consistent with non-covalent adsorption of COOH-microbeads or quenched CAT-microbeads and provide initial support to our conclusion that covalent attachment of microbeads can lead to increased persistence on model wound beds relative to adsorbed microbeads.

Figure 3G quantifies the density of CAT-microbeads (PS) and COOH-microbeads (PS) that persisted on the model wounds after the beads were incubated with the model wounds for three different time-periods. These results reveal that the density of attached CAT-microbeads (PS) increases with their time of incubation (upto 25X increase in 90 mins) relative to the control. This result thus provides evidence that the time of incubation of reactive beads on a model wound can be manipulated to vary the density of persistent beads.

We also used hydrolytically degradable beads made of 50:50 poly(lactic-co-glycolic acid) **(PLGA)** (diameter: 0.5 μm) in experiments similar to those as described above. The two different types of microbeads (PS versus PLGA) were employed to evaluate the generality of our approach. Figure 3H shows a data set obtained using degradable PLGA microbeads functionalized with catechol groups (CAT-microbeads (PLGA)). These results show that the density of attached CAT-microbeads (PLGA) is around 5 times greater than COOH-microbeads (PLGA) for both time-points (45 min and 90 min). Inspection of Figure 3F also reveals that catechol-functionalized PLGA beads can be immobilized on the surface of model wounds with densities of ~10^3 microbeads/mm^2. For PLGA beads with a diameter of 1 μm, if loaded with epidermal growth factor (EGF), this surface density of beads would permit the release of up to 10 ng/cm^2 (of tissue surface) of EGF over 15 days. Here we comment that past studies have shown that surface-immobilized EGF in the conc. range of 0.2–10 ng/cm^2 can promote a range of fundamental cell behaviors (e.g., migration) [30, 31, 44]. We conclude, therefore, that the results in Figure 3 provide support for our hypothesis that microbeads covalently immobilized on wounds beds can provide the basis of strategies for the release of biologically-relevant concentrations of growth factors from wound beds.

Finally, we note that a comparison of Figure 3G with Figure 3H reveals that the number of PLGA microbeads (Figure 3G and 3H: left axes) attached to porcine dermis is around 1.5–2 times that of PS microbeads. This difference may be due to differences in the surface density of carboxylate groups or the different diameters (PS – 1 μm vs PLGA – 0.5 μm) of the two types of microbeads. Significantly, however, the densities of attachment of both types of reactive microbeads are higher than controls, and the orders of magnitude of the attachment densities are similar (~10^2–10^3 microbeads/mm^2).

3.2 Covalent attachment of maleimide-functionalized microbeads to porcine dermis

Next, we examined the reaction of maleimide-functionalized microbeads (henceforth referred to as **MAL-microbeads**) with the surface of porcine dermis, as illustrated in Figure 1B. We selected the maleimide moeity as the basis of our second approach for covalent immobilization of microbeads on porcine dermis because maleimide chemistry has been used extensively for cross-linking of proteins via sulfhydryl groups (at physiological pH) [45]. Maleimide groups are relatively stable towards hydrolytic degradation [46, 47], and exhibit fast reaction kinetics (reactions are typically complete in less than an hour). These attributes make this chemistry potentially useful for enabling the interfacial engineering of wound bed in clinical settings.

We prepared **MAL-microbeads** by reacting amine-coated polystyrene microbeads (**NH_2-microbeads**) with the amine-reactive sulfo-succinimidyl group present at one end of sulfo-SMCC bifunctional crosslinker molecules (the other end has MAL-group) (see Figure 1B). During preparation of the functionalized microbeads, we measured the surface charge density of the polystyrene beads to decrease (NH_2-microbeads exhibited a ζ-potential of +17.4±1.5 mV and MAL-microbeads exhibited a ζ-potential of +3.4±0.8 mV in 1 mM MES buffer at pH 5.0), consistent with the replacement of amine groups (positively charged at pH 5.0) with maleimide groups (neutral at pH 5.0). We also prepared ‘quenched’ MAL-microbeads whose reactivity towards sulfhydryl groups was quenched by reaction in excess with BME overnight. The surface charge density of the MAL-microbeads after quenching was determined to remain unchanged.

In proteins found in native tissue, the sulfhydryl groups of cysteine are also present as disulfide bridges. We hypothesized that pretreatment of the porcine dermis with a mild reducing agent (that can reduce disulfide linkages) might, therefore, enable additional control over the covalent attachment of microbeads via maleimide chemistry (as illustrated in Figure 2B). In the experiments reported below, we investigated immobilization of MAL-

microbeads on porcine dermis samples with and without pretreatment with glutathione. Glutathione is a relatively mild reducing agent present in intracellular environments (concentration ranging from 1–11 mM) [48] and it has been used extensively as a non-toxic anti-oxidant [49]. Accordingly, we pretreated the porcine dermis samples with either glutathione (20 mM) in PBS (pH 7.4) or only PBS (control condition) for 30 minutes. Subsequently, the pre-treated porcine dermis samples were rinsed and incubated with suspensions of either MAL-microbeads, or quenched MAL-microbeads, or their precursor NH_2-microbeads for 30 minutes. After incubation with the microbeads, the porcine dermis samples were rinsed and incubated overnight in PBS to assess the persistence of the beads on the model wounds (see above for details).

Inspection of the fluorescent micrographs in Figure 4A–F reveals that MAL-microbeads exhibit a pronounced increase in persistence on the porcine dermis samples relative to their precursor NH_2-microbeads or quenched MAL-microbeads, both with and without glutathione pretreatment. These images also reveal that the maleimide-functionalized beads attach in a largely non-aggregated state (see Figure S4). Figure 4G quantifies the density of attachment, and reveals that the density of the maleimide-functionalized PS beads on the porcine dermis sample is nearly 20-fold higher than the amine-coated beads. Several additional conclusions are also evident from inspection of Figure 4. First, maleimide-functionalized PS beads (Figure 4G) and maleimide-functionalized PLGA beads (Figure 4H) show a similar trend in their persistence after incubation in PBS (higher density relative to their non-functionalized counterparts), indicating that the choice of polymeric material and microbead size did not significantly affect the covalent attachment of the reactive beads or their persistence. Second, as also shown in Figures 4G and 4H, the density of attachment of the MAL-microbeads (made of either PS or PLGA) to porcine dermis was increased by almost two-fold by the pre-treatment of porcine dermis with glutathione. This result supports our proposal that control over the density of attachment of maleimide-functionalized microbeads can be achieved via pre-treatment of model wound-beds with glutathione.

Thirdly, the density of attachment of quenched MAL-microbeads was also much lower (nearly 70% less) than MAL-microbeads, consistent with the higher attachment density of MAL-microbeads being due to the covalent reactivity of the MAL-microbeads. An additional result that is evident in Figure 4G is that the density of quenched MAL-microbeads on the porcine dermis sample is higher than the NH_2-microbeads (although both densities are much lower than MAL-microbeads). Specifically, the density of attachment of quenched MAL-microbeads was 2–3 times higher than NH_2-microbeads. We hypothesized that the difference between MAL-microbeads and NH_2-microbeads was likely a result of differences in physical interactions of the two types of microbeads with the porcine dermis sample. To explore this hypothesis, we measured the zeta-potentials of the microbeads in 1 mM PBS at pH 7.4, the conditions used to test persistence of the beads on the surface of the porcine dermis. These measurements revealed the zeta potentials to be -11.7 ± 0.9 mV for the NH_2-microbeads and -26.6 ± 2.4 mV for quenched MAL-microbeads (the latter measurement is similar to that measured for the MAL-microbeads; -25.5 ± 1.7 mV). We conclude, therefore, that the MAL-microbeads (quenched) have a substantially higher surface charge density than the NH_2-microbeads. This higher charge density may be the cause of the greater density of quenched MAL-microbeads on the porcine dermis sample, as compared to the NH_2-microbeads. We also comment that the origin of the negative zeta potentials measured at pH 7.4 is likely residual carboxylic acid groups that, according to the supplier of the microbeads (Invitrogen, Carlsbad, CA), are present on the surface of the microbeads. Consistent with this explanation, as mentioned earlier in this section, at pH values of 5.0, we had measured the zeta-potentials of the NH_2-microbeads and MAL-microbeads to be $+17.4\pm1.5$ mV and $+3.4\pm0.8$ mV, respectively. The dependence of the zeta

potential of the microbeads on pH appears to be influenced by protonation of both the amine and COO^- groups on the surface of the beads.

3.3 Raman microspectroscopy of porcine dermis

The results described above support our proposition that native functional groups presented by porcine dermis can be used to covalently immobilize reactive microbeads. To provide additional support for this conclusion, we next characterized the surface chemical composition of porcine dermis by using Raman microspectroscopy with the specific goal of finding evidence of the availability of sulfhydryl and amine groups for covalent bond formation. We also sought to use Raman microspectroscopy to provide additional evidence for covalent reaction of maleimide groups with sulfhydryl groups on the wound bed. Our approach was motivated by past studies that have used near-IR excited Raman spectroscopy for molecular characterization of full-thickness skin [50, 51], and other biological tissues (such as brain, colon, liver, muscle) [52]. In those past studies, spectral bands were assigned to biochemical components such as protein, lipid, water and disulfide bonds.

The Raman spectrum of porcine dermis (averaged over multiple samples) obtained in our investigation is presented in Figure 5 along with peak assignments [51, 53, 54]. Here we note that attempts to find direct evidence of free amine (-NH_2: vibrational peak - 3250–3300 cm^{-1} [55]) or free sulfhydryl (-SH: vibrational peak – 2560–2590 cm^{-1}) groups on the surface of porcine dermis samples were not successful due to attenuation of the signal at high wavenumbers (beyond 2400 cm^{-1}). Thus, as described below the presence of these functional groups was necessarily inferred from other Raman spectroscopic signatures. For example, the spectrum in Figure 5 clearly indicates a surface rich in collagen (α-helix peaks at 1660 cm^{-1} (amide I) and 1269 cm^{-1} (amide III)). The strong band at 939 cm^{-1} has been assigned to the presence of α-helical proteins [56]. Additionally, the presence of elastin is evidenced by a peak at 1340 cm^{-1} [57] and the peaks at 528 cm^{-1} are due to disulfide linkages in elastin [58, 59]. Finally, lipids in a fluid state are indicated by the broad peak at 1100 $cm.^{-1}$ [56]. Overall, the spectrum in Figure 5 is generally indicative of a surface with a high abundance of proteins. Such a protein-rich surface would be expected to present–NH_2 groups for attachment of amine-reactive functionalized microbeads (CAT-microbeads).

Inspection of Figure 5 reveals additionally that the 1660/1452 cm^{-1} peak intensity ratio is 0.69. This ratio has been previously used to infer the relative amounts of collagen and total protein [60]. Briefly, since the peak at 1660 cm^{-1} is attributed to the α-helices in collagen fibrils, while the peak at 1452 cm^{-1} is attributed to CH_2-scissoring present in all proteins (including collagen), the ratio of the two peak intensities can be used to estimate the quantity of other proteins relative to collagen. Type I collagen is not cysteine-rich and has only a few disulfide linkages. However, other proteins (e.g. Type III collagen, elastin, fibrinogen) and their precursors (e.g. tropoelastin and procollagen) are rich in disulfides and cysteines. Thus, we indirectly infer also the availability of cysteinyl sulfhydryl groups for covalent linkage on the surface of porcine dermis.

Next, we measured the Raman spectrum of porcine dermis treated with reactive sulfo-SMCC crosslinker or that treated with quenched sulfo-SMCC - quenched either with only Tris-HCl (to form Tris-maleimide), or with both Tris-HCl and β-mercaptoethanol (see Table 1). Control dermis samples treated with only Tris-HCl or β-mercaptoethanol were also examined. Maleimides have a very strong peak at 1766 cm^{-1} (Figure S1) in their Raman spectra due to the symmetric stretch of the cyclic imide moiety [61]. We hypothesized that the cyclic imide, which remains intact after reaction with a sulfhydryl group, would retain its Raman spectra peak after covalent bond formation. Here we note that the succinimide moiety in sulfo-SMCC is also a cyclic imide (peak at 1766 cm^{-1}) and is capable of forming a covalent bond with free amines on porcine dermis. Hence, one of our controls was sulfo-

SMCC whose amine-reactive sulfo-succinimide was quenched by reaction overnight with Tris-HCl (containing 1 amine group/molecule).

Following the 30 min treatment of the porcine dermis with fresh sulfo-SMCC (both maleimide and succinimide groups are present and reactive), sulfo-SMCC quenched with Tris-HCl (Tris-maleimide) and sulfo-SMCC quench with Tris-HCl and β-mercaptoethanol (Figure 6: Control 1) (see Table 1 for details), we incubated the samples overnight in PBS before measuring the Raman spectra. Inspection of Figure 6 reveals evidence of the immobilization of the maleimide group (see peak at 1766 cm^{-1}) on only those porcine dermis samples that were treated with reagents containing reactive maleimide groups, i.e. (1) sulfo-SMCC, and (2) sulfo-SMCC quenched with Tris-HCl. This implicitly supports our conclusion that free sulfhydryl groups on porcine dermis samples are accessible to reactive maleimide groups. Here we note that attempts to find evidence of a covalent reaction between catechols and porcine dermis were not successful due to the inherently weak spectra of catechols relative to back ground signals from the porcine dermis.

3.4 Covalent attachment of degradable maleimide-functionalized microbeads on excisional dermal wounds in live mice in vivo

As described in the Introduction, the long-term goal of the research described in this paper is to explore the hypothesis that reactive microbeads can be covalently immobilized on wound-beds in a clinical setting to accelerate wound healing. As an additional step toward achieving that goal, we functionalized fluorescent, degradable microbeads (PLGA; diameter: 0.5 μm.) with maleimide groups (as described above) and applied them to full-thickness dermal wounds to determine if covalent attachment of the beads on wounds could be achieved. Four mm diameter wounds were surgically created on the flanks of live mice using biopsy punches. Because lipids are generally found in the subcutaneous tissue of diabetic mice in high quantities [62], we compared the attachment of MAL-microbeads to full-thickness dermal wound beds in diabetic (db/db) and wild-type mice. We sought to determine if differences in the relative protein (and hence sulfhydryl groups) and lipid content of the wound-beds would be evidenced in the relative density of immobilization of microbeads on their surfaces.

After incubation of MAL-microbeads on the wounds of the mice for 30 mins, the wounds were rinsed with excess PBS (pH 7.4) several times. Subsequently, the mice were euthanized and the wounds were harvested. The harvested wounds were imaged using fluorescence microscopy. Inspection of Figure 7 reveals that we indeed measured higher attachment densities of MAL-microbeads, relative to their precursor NH_2-microbeads, on the harvested wounds of wild-type mice (see Figure 7A–B). Interestingly, we also observed a heterogeneous distribution of microbeads attached to the wound bed, hinting at the presence of localized regions on the wound bed that have greater availability of reactive cysteine-groups. We also note that the attachment of the non-reactive, charged precursor beads on the wound beds was also heterogeneous, which may reflect (i) topographic heterogeneity on the surface of the wound bed, causing microbeads to get entrapped in the grooves, and/or (ii) heterogeneity in the physical properties of the wound bed (e.g., differences in the density of surface charge on the wound bed).

In comparison to the wild-type mice (see Figure 7D), we observed a significantly lower density of MAL-microbeads attachment in wound-beds of diabetic mice (see Figure 7C). This indicates that fresh full-thickness wounds in diabetic mice present native chemical functionality that is distinct relative to wild-type mice. Some possible origins of these observed differences are (i) a high lipid content in the subcutaneous tissue of diabetic mice, as reported previously [62], and (ii) a low availability of amine groups due to high levels of glycosylation generally seen in diabetic tissue [63]. We comment that it is also known that

there is an impaired healing response to wounding (including protein secretion) in diabetic animals [64] which likely also results in lower secretion of cysteine-rich precursor peptides and proteins. In future studies, we plan to compare the attachment of MAL-microbeads in diabetic and wild-type wounds with granulation beds to investigate differences in the quantity of secreted pre-cursor peptides and proteins. We also note that low densities of attached non-reactive microbeads (control) on the diabetic wound bed relative to wound beds in normal mice suggests that the proteins present on wound beds mediate physical interactions with the microbeads (such as through charged groups). We conclude these observations by commenting that, in addition to their potential use as a delivery vehicle for growth factors, we interpret the results above to also indicate that reactive microbeads in general, might form the basis of a general methodology that can be used to map the presentation of native chemical functional groups in wound beds *in vivo*. Such information has the potential to guide the design of vehicles for the spatially controlled delivery of drugs to wound beds.

3.5 Influence of maleimide-functionalized microbeads on healing of live mice wounds in vivo

The results above demonstrate that covalently reactive microbeads can be immobilized in mice wounds *in vivo*. In the context of wound healing, however, because maleimide groups are reactive, we considered it a possibility that the reaction of the maleimide-functionalized beads with the wound bed might impair wound healing [65]. To address this question, we immobilized non-fluorescent MAL-microbeads (PLGA, diameter – 0.5 μm) on 'splinted' wounds of wild-type mice and tracked the healing of the wounds over time until their closure. 'Splinted' wounds refer to the incorporation of 'O-ring splints' around the wound area which increases granulation tissue formation in the wounds, promotes healing by re-epithelialization rather than contracture and thus more accurately models human wound healing [66]. The wounds were incubated with 100 μL of a suspension of microbeads (reactive and non-reactive control; concentration: ~7×10^9 microbeads/mL) for 30 mins. Figure 8 summarizes the rate of wound closure as a function of time.

Inspection of Figure 8 reveals no difference in the rate of wound closure between the different sets of mice wounds that were either treated with MAL-microbeads or NH_2-microbeads or untreated. Statistical analysis (one-way ANOVA) confirmed that no significant differences exist in the mean wound size between the three data groups on any day. Here we note that our experimental approach does not involve placement of small molecule cross-linkers on the wound bed, but rather microbeads functionalized with reactive maleimide groups were contacted with the wound. The relative toxicity of molecular and microbead-sized cross-linkers is unknown, and will be the subject of future investigation.

In future studies, we plan to covalently attach degradable microbeads that encapsulate cyto-active factors or antimicrobial agents to model wound beds *in vivo*, and to use that capability to engineer wound beds to deliver biochemical cues to promote wound healing. In addition, we note that appropriately sized non-degradable microbeads could be used to alter the mechanical stiffness and topography of wound beds. Such approaches are also promising ones for cueing cell behaviors that accelerate the healing of wounds.

CONCLUSIONS

We have shown that wound beds present native chemical functional groups that can be utilized for the covalent attachment of polymeric microbeads (degradable and non-degradable). Specifically, we have shown that microbeads that are functionalized to be reactive towards amine and sulfhydryl groups can be covalently immobilized on model *ex vivo* and *in vivo* wound beds at controlled densities. A key result is that the covalently

attached microbeads are persistent relative to non-reactive microbeads when subjected to rinsing simulating wound exudate. Complementary experiments performed using Raman microspectroscopy provide additional support for our conclusions regarding covalent immobilization of maleimide-containing molecules and suggest, more broadly, that Raman microspectroscopy could be a useful tool to characterize the surface chemistry/reactivity of different wound bed types. We also demonstrated the feasibility of using covalent immobilization strategies with live mice wounds, and observed differential levels of immobilization of maleimide-functionalized beads on wild-type and diabetic wounds, consistent with anticipated differences in the presentation of amine and sulfhydryl groups at the surfaces of the two types of wound beds *in vivo*. Overall, the results of this study enable the use of covalent chemistry to immobilize microbeads directly onto wound beds to promote accelerated wound healing.

Supplementary Material

Refer to Web version on PubMed Central for supplementary material.

Acknowledgments

The authors thank Kathleen M. Guthrie, Kevin W. Johnson, Dana S. Tackes, and Allison R. Clarke for assistance with mice studies. The funding for this study was provided by NIH grant 1RC2AR058971-01 from NIAMS and an Innovation & Economic Development Research grant from the University of Wisconsin-Madison Graduate School. A.A. acknowledges fellowship support from the Ewing Marion Kauffman Foundation. Supporting Information is available online or from the authors. AA, MJS, CJM, JFM, and NLA possess financial interests in Wound Engineering LLC and/or Imbed Biosciences Inc., for-profit organizations that have filed patent applications and/or are commercializing aspects of the work reported in this publication.

References

1. Sweitzer SM, Fann SA, Borg TK, Baynes JW, Yost MJ. What is the future of diabetic wound care? Diabetes Educator. 2006; 32:197–210. [PubMed: 16554422]
2. Werner S, Grose R. Regulation of wound healing by growth factors and cytokines. Physiol Rev. 2003; 83:835–870. [PubMed: 12843410]
3. Biggs MJP, Richards RG, Dalby MJ. Nanotopographical modification: a regulator of cellular function through focal adhesions. Nanomed-Nanotechnol. 2010; 6:619–633.
4. Liliensiek SJ, Wood JA, Yong JA, Auerbach R, Nealey PF, Murphy CJ. Modulation of human vascular endothelial cell behaviors by nanotopographic cues. Biomaterials. 2010; 31:5418–5426. [PubMed: 20400175]
5. Pot SA, Liliensiek SJ, Myrna KE, Bentley E, Jester JV, Nealey PF, et al. Nanoscale topography-induced modulation of fundamental cell behaviors of rabbit corneal keratocytes, fibroblasts, and myofibroblasts. Invest Ophth Vis Sci. 2010; 51:1373–1381.
6. Hinz B. The myofibroblast: paradigm for a mechanically active cell. J Biomech. 2010; 43:146–155. [PubMed: 19800625]
7. Chien S, Li S, Shiu YT, Li YS. Molecular basis of mechanical modulation of endothelial cell migration. Front Biosci. 2005; 10:1985–2000. [PubMed: 15769679]
8. Baker EL, Zaman MH. The biomechanical integrin. J Biomech. 2010; 43:38–44. [PubMed: 19811786]
9. Senet P, Vicaut E, Beneton N, Debure C, Lok C, Chosidow O. Topical treatment of hypertensive leg ulcers with platelet-derived growth factor-BB: a randomized controlled trial. Arch Dermatol. 2011; 147:926–930. [PubMed: 21482863]
10. Landsman A, Agnew P, Parish L, Joseph R, Galiano RD. Diabetic foot ulcers treated with becaplermin and theragauze a moisture-controlling smart dressing: a randomized, multicenter, prospective analysis. J Am Podiat Med Assn. 2010; 100:155–160.
11. Bello YM, Phillips TJ. Recent advances in wound healing. Jama-J Am Med Assoc. 2000; 283:716–718.

12. Schultz GS, Sibbald RG, Falanga V, Ayello EA, Dowsett C, Harding K, et al. Wound bed preparation: a systematic approach to wound management. Wound Repair Regen. 2003; 11:S1–S28. [PubMed: 12654015]
13. Falanga V, Grinnell F, Gilchrest B, Maddox YT, Moshell A. Workshop on the pathogenesis of chronic wounds. J Invest Dermatol. 1994; 102:125–127. [PubMed: 8288905]
14. Dworniczek E, Nawrot U, Seniuk A, Wlodarczyk K, Bialynicki-Birula R. The in vitro Effect of a silver-containing dressing on biofilm development. Adv Clin Exp Med. 2009; 18:277–281.
15. Mooney EK, Lippitt C, Friedman J. Plastic Surg Ed Fdn DC. Silver dressings. Plast Reconstr Surg. 2006; 117:666–669. [PubMed: 16462356]
16. Atiyeh BS, Costagliola M, Hayek SN, Dibo SA. Effect of silver on burn wound infection control and healing: review of the literature. Burns. 2007; 33:139–148. [PubMed: 17137719]
17. Dunn K, Edwards-Jones V. The role of Acticoat (TM) with nanocrystalline silver in the management of burns. Burns. 2004; 30:S1–S9. [PubMed: 15327800]
18. Lee K, Silva EA, Mooney DJ. Growth factor delivery-based tissue engineering: general approaches and a review of recent developments. J Roy Soc Interface. 2011; 8:153–170. [PubMed: 20719768]
19. Richardson TP, Peters MC, Ennett AB, Mooney DJ. Polymeric system for dual growth factor delivery. Nat Biotechnol. 2001; 19:1029–1034. [PubMed: 11689847]
20. Jaklenec A, Hinckfuss A, Bilgen B, Ciombor DM, Aaron R, Mathiowitz E. Sequential release of bioactive IGF-I and TGF-beta(1) from PLGA microsphere-based scaffolds. Biomaterials. 2008; 29:1518–1525. [PubMed: 18166223]
21. DeFail AJ, Chu CR, Izzo N, Marra KG. Controlled release of bioactive TGF-beta(1) from microspheres embedded within biodegradable hydrogels. Biomaterials. 2006; 27:1579–1585. [PubMed: 16140372]
22. Chen FM, Zhao YM, Sun HH, Jin T, Wang QT, Zhou W, et al. Novel glycidyl methacrylated dextran (Dex-GMA)/gelatin hydrogel scaffolds containing microspheres loaded with bone morphogenetic proteins: formulation and characteristics. J Control Release. 2007; 118:65–77. [PubMed: 17250921]
23. Schmidt CE, Dai JW, Lauffenburger DA, Sheetz MP, Horwitz AF. Integrin-cytoskeletal interactions in neuronal growth cones. J Neurosci. 1995; 15:3400–3407. [PubMed: 7751919]
24. Saperia D, Glassberg E, Lyons RF, Abergel RP, Baneux P, Castel JC, et al. Demonstration of elevated type-I and type-III procollagen messenger-RNA levels in cutaneous wounds treated with Helium-Neon laser – proposed mechanism for enhanced wound-healing. Biochem Bioph Res Co. 1986; 138:1123–1128.
25. Ashcroft GS, Kielty CM, Horan MA, Ferguson MWJ. Age-related changes in the temporal and spatial distributions of fibrillin and elastin mRNAs and proteins in acute cutaneous wounds of healthy humans. J Pathol. 1997; 183:80–89. [PubMed: 9370952]
26. Grinnell F, Billingham RE, Burgess L. Distribution of fibronectin during wound-healing in vivo. J Invest Dermatol. 1981; 76:181–189. [PubMed: 7240787]
27. Nguyen BP, Ryan MC, Gil SG, Carter WG. Deposition of laminin 5 in epidermal wounds regulates integrin signaling and adhesion. Curr Opin Cell Biol. 2000; 12:554–562. [PubMed: 10978889]
28. Houghton, AM.; Mouded, M.; Shapiro, SD. Consequences of elastolysis. In: Parks, WC.; Mecham, RP., editors. Extracellular matrix degradation. Berlin: Springer-Verlag Inc.; 2011. p. 217-249.
29. Prockop DJ, Kivirikko KI. Collagens – molecular-biology, diseases, and potentials for therapy. Ann Rev Biochem. 1995; 64:403–434. [PubMed: 7574488]
30. Puccinelli TJ, Bertics PJ, Masters KS. Regulation of keratinocyte signaling and function via changes in epidermal growth factor presentation. Acta Biomater. 2010; 6:3415–3425. [PubMed: 20398806]
31. Stefonek-Puccinelli TJ, Masters KS. Co-immobilization of gradient-patterned growth factors for directed cell migration. Ann Biomed Eng. 2008; 36:2121–2133. [PubMed: 18850272]
32. Ashcroft GS, Yang X, Glick AB, Weinstein M, Letterio JJ, Mizel DE, et al. Mice lacking Smad3 show accelerated wound healing and an impaired local inflammatory response. Nat Cell Biol. 1999; 1:260–266. [PubMed: 10559937]
33. Greenhalgh DG, Sprugel KH, Murray MJ, Ross R. PDGF and FGF stimulate wound-healing in the genetically diabetic mouse. Am J Pathol. 1990; 136:1235–1246. [PubMed: 2356856]

34. Sullivan TP, Eaglstein WH, Davis SC, Mertz P. The pig as a model for human wound healing. Wound Repair Regen. 2001; 9:66–76. [PubMed: 11350644]
35. Reisner LA, Cao A, Pandya AK. An integrated software system for processing, analyzing, and classifying Raman spectra. Chemometr Intell Lab. 2011; 105:83–90.
36. Guthrie KM, Agarwal A, Tackes DS, Johnson KW, Abbott NL, Murphy CJ, et al. Antibacterial efficacy of silver-impregnated polyelectrolyte multilayers immobilized on a biological dressing in a murine wound infection model. Ann Surg. 2012; 256(2):371–377. [PubMed: 22609841]
37. Lee H, Dellatore SM, Miller WM, Messersmith PB. Mussel-inspired surface chemistry for multifunctional coatings. Science. 2007; 318:426–430. [PubMed: 17947576]
38. Lee H, Rho J, Messersmith PB. Facile conjugation of biomolecules onto surfaces via mussel adhesive protein inspired coatings. Adv Mater. 2009; 21:431–434. [PubMed: 19802352]
39. Lee H, Lee BP, Messersmith PB. A reversible wet/dry adhesive inspired by mussels and geckos. Nature. 2007; 448 338-U4.
40. Gademann K, Kobylinska J, Wach JY, Woods TM. Surface modifications based on the cyanobacterial siderophore anachelin: from structure to functional biomaterials design. Biometals. 2009; 22:595–604. [PubMed: 19350397]
41. Waite JH. Surface chemistry - Mussel power. Nat Mater. 2008; 7:8–9. [PubMed: 18167496]
42. Schweigert N, Zehnder AJB, Eggen RIL. Chemical properties of catechols and their molecular modes of toxic action in cells, from microorganisms to mammals. Environ Microbiol. 2001; 3:81–91. [PubMed: 11321547]
43. Land, EJ.; Ramsden, CA.; Riley, PA. Quinones and Quinone Enzymes, Pt A. San Diego: Academic Press Inc; 2004. Quinone chemistry and melanogenesis; p. 88-109.
44. Stefonek TJ, Masters KS. Immobilized gradients of epidermal growth factor promote accelerated and directed keratinocyte migration. Wound Repair Regen. 2007; 15:847–855. [PubMed: 18028133]
45. Wu CW, Yarbrough LR, Wu FYH. N-(1-pyrene)maleimide - fluorescent cross-linking reagent. Biochemistry-US. 1976; 15:2863–2868.
46. Yoshitake S, Yamada Y, Ishikawa E, Masseyeff R. Conjugation of glucose-oxidase from Aspergillus-niger and rabbit antibodies using N-hydroxysuccinimide ester of N-(4-carboxycyclohexylmethyl)-maleimide. Eur J Biochem. 1979; 101:395–399. [PubMed: 574817]
47. Hermanson, GT. Bioconjugate Techniques. 2nd Edition ed. London, UK: Academic Press; 2008. The chemistry of reactive groups; p. 183-184.
48. Valko M, Leibfritz D, Moncol J, Cronin MTD, Mazur M, Telser J. Free radicals and antioxidants in normal physiological functions and human disease. Int J Biochem Cell B. 2007; 39:44–84.
49. Sen CK. Redox signaling and the emerging therapeutic potential of thiol antioxidants. Biochem Pharmacol. 1998; 55:1747–1758. [PubMed: 9714292]
50. Caspers PJ, Lucassen GW, Wolthuis R, Bruining HA, Puppels GJ. In vitro and in vivo Raman spectroscopy of human skin. Biospectroscopy. 1998; 4:S31–S9. [PubMed: 9787912]
51. Greve TM, Andersen KB, Nielsen OF. ATR-FTIR, FT-NIR and near-FT-Raman spectroscopic studies of molecular composition in human skin in vivo and pig ear skin in vitro. Spectrosc-Int J. 2008; 22:437–457.
52. Krafft, C. Vibrational spectroscopic imaging of soft tissue. In: Salzer, R.; Siesler, HW., editors. Infrared and Raman Spectroscopic Imaging. Weinheim, Germany: Wiley-VCH Verlag GmbH & Co. KGaA; 2009. p. 113-147.
53. Barry BW, Edwards HGM, Williams AC. Fourier-transform raman and infrared vibrational study of human skin – assignment of spectral bands. J Raman Spectrosc. 1992; 23:641–645.
54. Naito S, Min YK, Sugata K, Osanai O, Kitahara T, Hiruma H, et al. In vivo measurement of human dermis by 1064 nm-excited fiber Raman spectroscopy. Skin Res and Technol. 2008; 14:18–25. [PubMed: 18211598]
55. Edwards, H. Spectra-structure correlations in Raman spectroscopy. In: Chalmers, J.; Griffiths, P., editors. Handbook of Vibrational Spectroscopy. John Wiley and Sons; 2002. p. 1838-1871.
56. Gniadecka M, Nielsen OF, Christensen DH, Wulf HC. Structure of water, proteins, and lipids in intact human skin, hair, and nail. J Invest Dermatol. 1998; 110:393–398. [PubMed: 9540981]

57. Baraga JJ, Feld MS, Rava RP. Insitu optical histochemistry of human artery using near-infrared fourier-transform raman-spectroscopy. P Natl Acad Sci USA. 1992; 89:3473–3477.
58. Frushour BG, Koenig JL. Raman-scattering of collagen, gelatin, and elastin. Biopolymers. 1975; 14:379–391. [PubMed: 1174668]
59. Debelle L, Alix AJP, Jacob MP, Huvenne JP, Berjot M, Sombret B, et al. Bovine elastin and kappa-elastin secondary structure determination by optical spectroscopies. J Biol Chem. 1995; 270:26099–26103. [PubMed: 7592811]
60. Crane NJ, Brown TS, Evans KN, Hawksworth JS, Hussey S, Tadaki DK, et al. Monitoring the healing of combat wounds using Raman spectroscopic mapping. Wound Repair Regen. 2010; 18:409–416. [PubMed: 20546554]
61. McKittrick PT, Katon JE. Infrared and raman group frequencies of cyclic imides. Appl Spectrosc. 1990; 44:812–817.
62. Coleman DL. Diabetes-obesity syndromes in mice. Diabetes. 1982; 31:1–6. [PubMed: 7160533]
63. Brownlee M. Advanced protein glycosylation in diabetes and aging. Annu Rev Med. 1995; 46:223–234. [PubMed: 7598459]
64. Werner S, Breeden M, Hubner G, Greenhalgh DG, Longaker MT. Induction of keratinocyte growth-factor expression is reduced and delayed during wound-healing in the genetically diabetic mouse. J Invest Dermatol. 1994; 103:469–473. [PubMed: 7930669]
65. Uehara Y, Fisher JM, Rabinovitz M. Showdomycin and its reactive moiety, maleimide – a comparison in selective toxicity and mechanism of action invitro. Biochem Pharmacol. 1980; 29:2199–2204. [PubMed: 7426025]
66. Galiano RD, Michaels J, Dobryansky M, Levine JP, Gurtner GC. Quantitative and reproducible murine model of excisional wound healing. Wound Repair Regen. 2004; 12:485–492. [PubMed: 15260814]

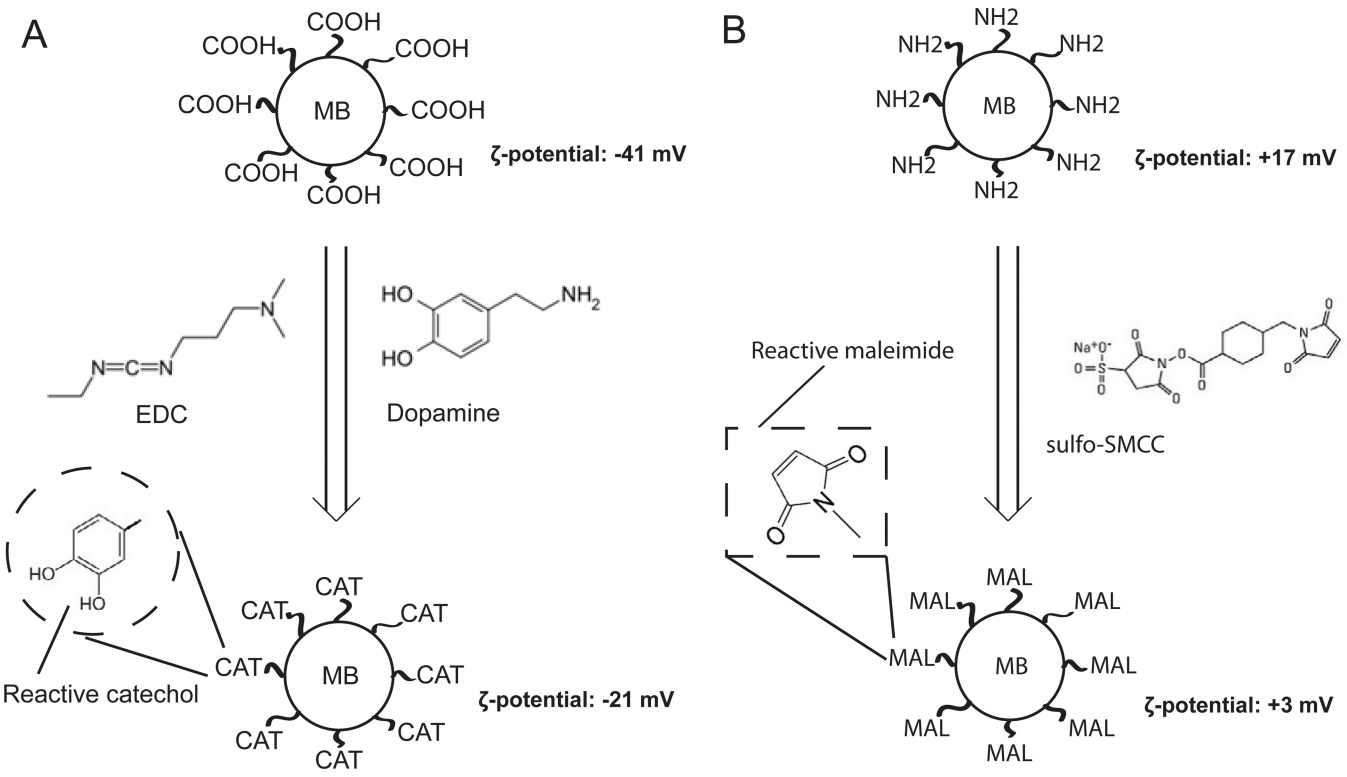

Figure 1.

(A) Carboxylate-modified polystyrene microbeads (MB) were functionalized with catechol by reaction of the surface carboxylic acids with the amine groups of dopamine using EDC as a cross-linker (pH 5.0, 2 hrs). ζ-potential was measured in 1 mM PBS (pH 7.4) (B) Amine-modified polystyrene microbeads were functionalized with maleimide groups by reaction with the sulfo-succinimidyl moeity of sulfo-SMCC cross-linker (pH 7.4, 30 mins). ζ-potential was measured in 1 mM MES buffer (pH 5.0).

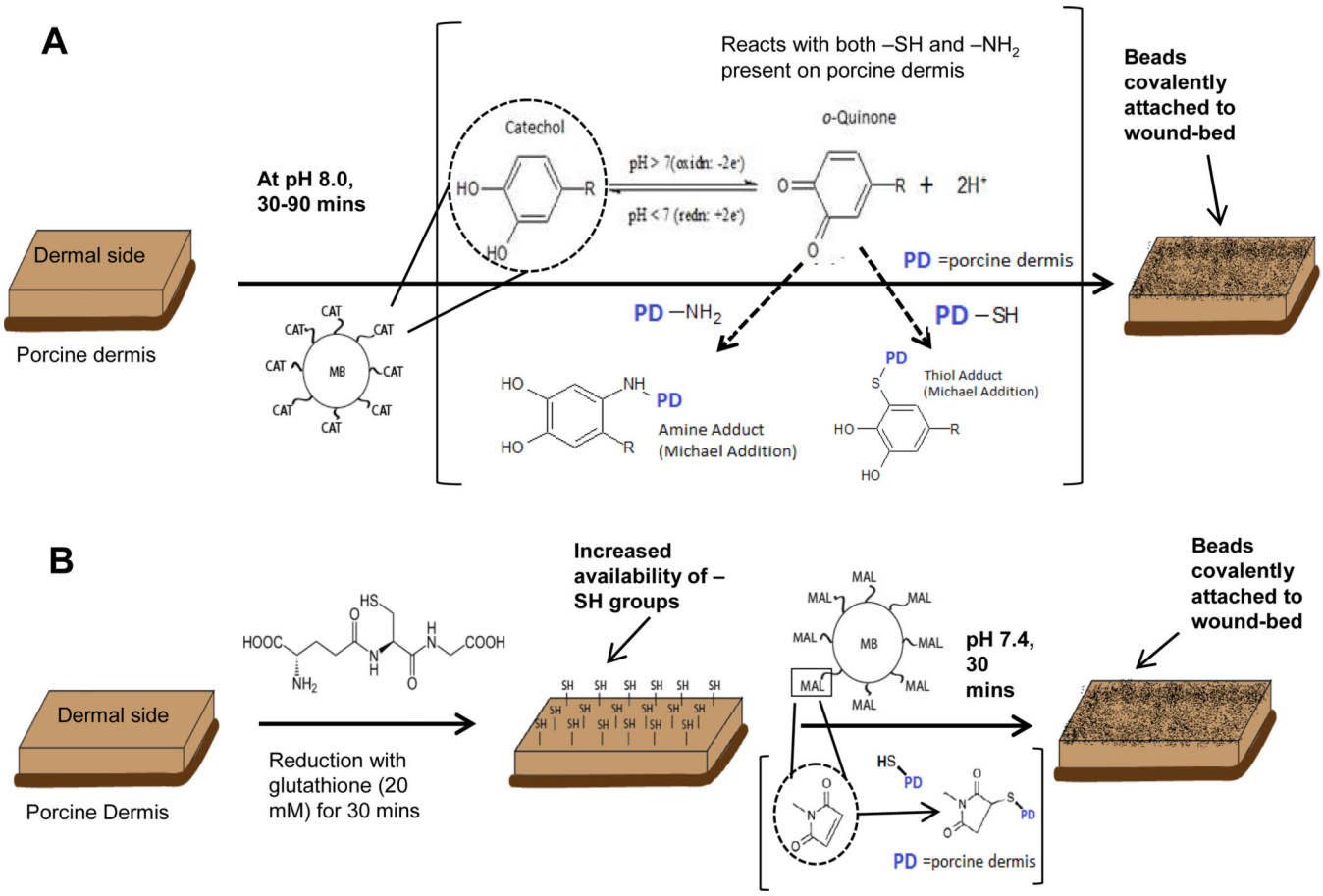

Figure 2.

(A) Porcine dermis (PD) was treated with reactive catechol-functionalized microbeads (MB-CAT) at physiologic pH (pH 7.4), followed by overnight incubation in PBS on shaker. (B) PD samples were treated with a mild reducing agent (glutathione – 20 mM.) to increase the availability of sulfhydryl groups for covalent attachment with maleimide functionalized microbeads (MB-MAL). Subsequently, MB-MAL were incubated for 30 mins followed by overnight incubation in PBS on a shaker.

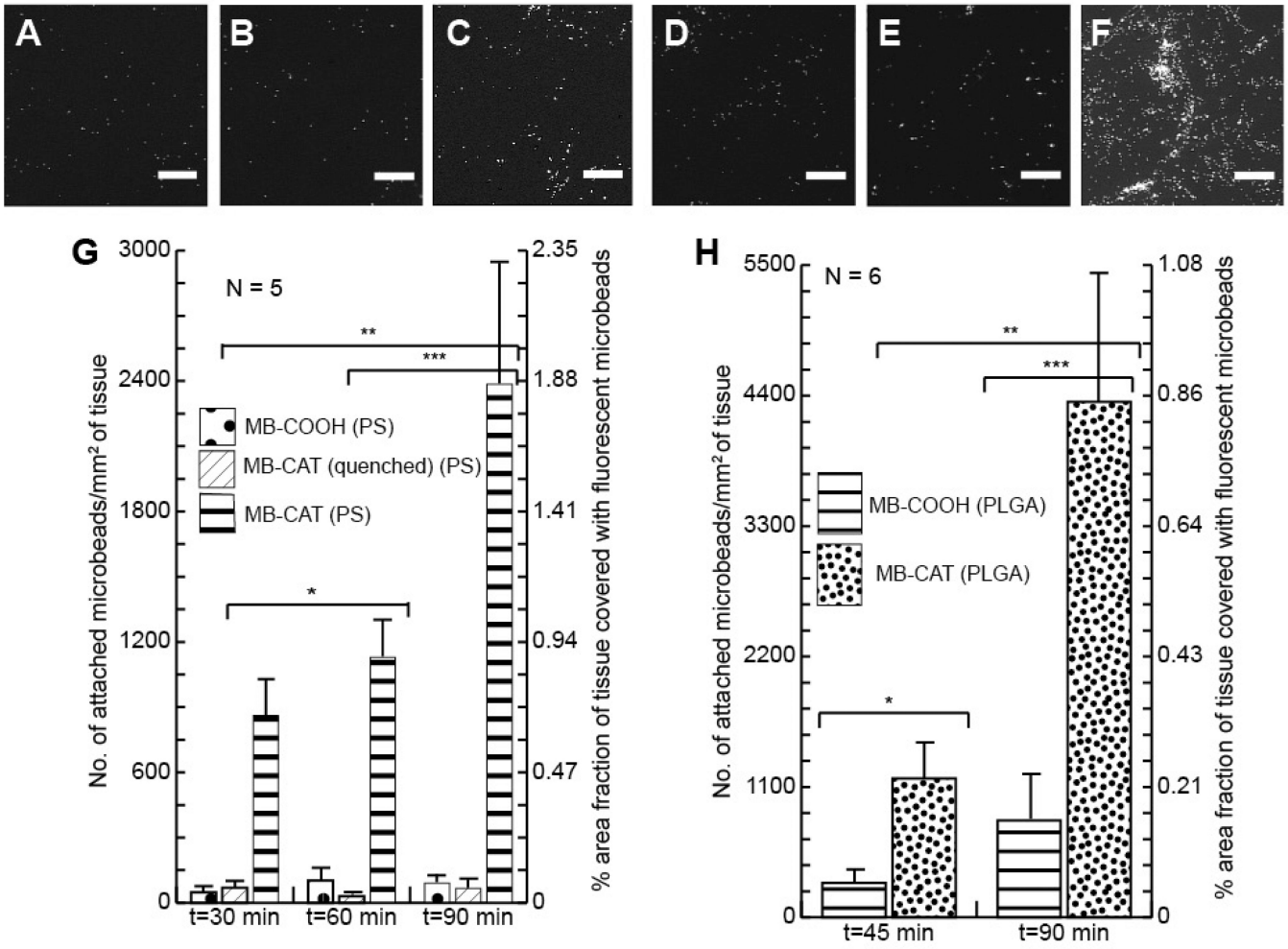

Figure 3.

[A]–[F]: Fluorescence microscopy images of porcine dermis (PD) samples treated with different fluorescent polystyrene microbeads [A] MB-COOH (30 mins), [B] MB-CAT(quenched) (30 mins), [C] MB-CAT (30 mins), [D] MB-COOH (90 mins), [E] MB-CAT(quenched) (90 mins), [F] MB-CAT (90 mins). [G] and [H] are graphs for the quantitative comparison of microbead attachment to PD treated with different sets of microbeads for different times. ([G] – 1 μm. polystyrene MBs and [H] – 0.5 μm PLGA MBs). Asterisks (*, **, ***) indicate statistically significant difference ($\alpha<0.05$) between compared sample sets. Scale bars: 100 μm

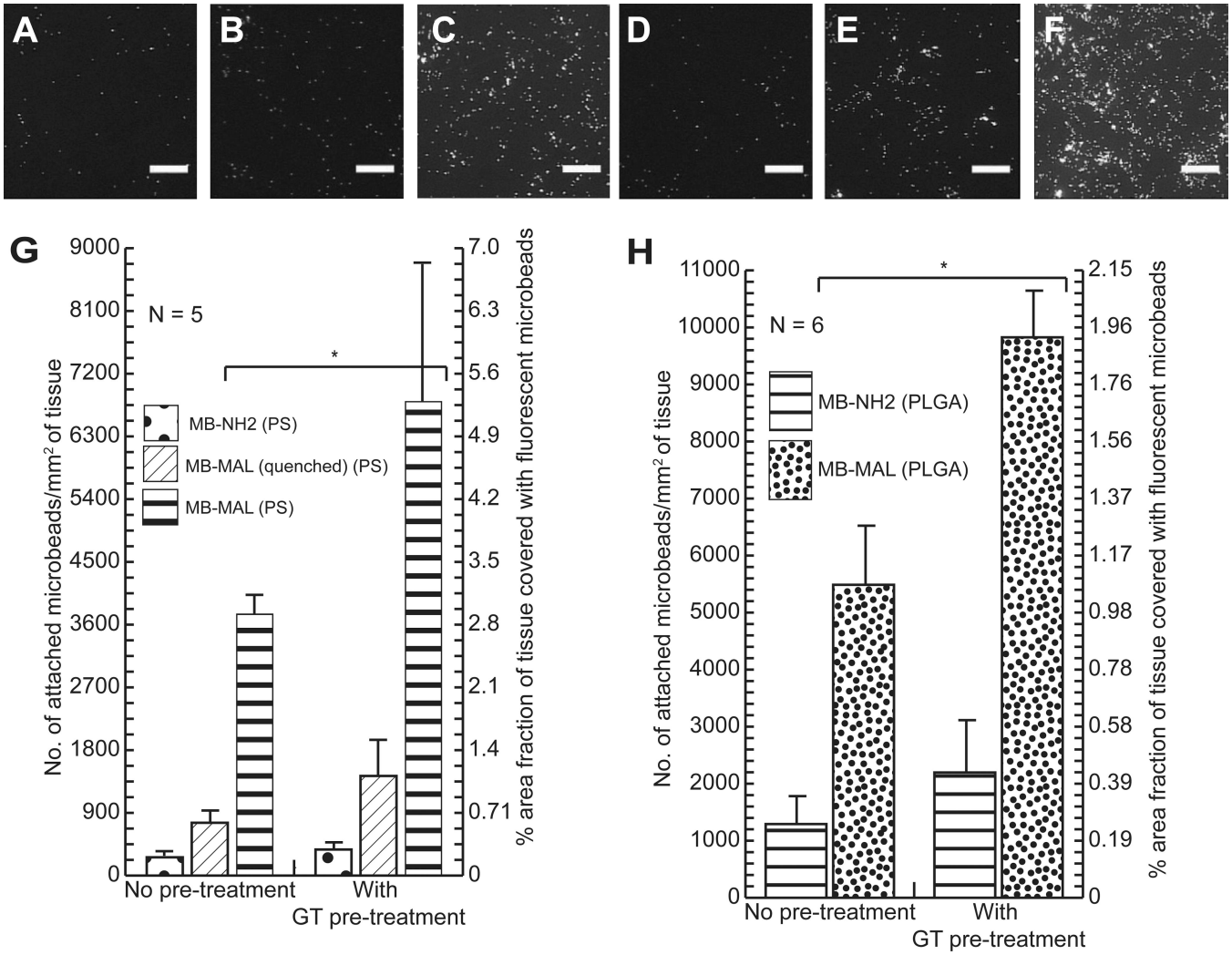

Figure 4.

[A]–[F] Fluorescence microscopy images of porcine dermis (PD) samples treated for 30 mins. with different fluorescent polystyrene microbeads. [D]–[F] were pre-treated with glutathione ((GT), 20 mM.) while [A]–[C] were not. [A, D] were treated with NH_2-microbeads, [B, E] were treated with MAL-microbeads (quenched), and [C,F] were treated with MAL-microbeads. [G] and [H] are graphs for the quantitative comparison of microbead attachment to PD samples treated with different sets of microbeads under different conditions ([G] – 1 μm polystyrene MBs and [F] – 0.5 μm PLGA MBs). Asterisk (*) indicates statistically significant difference ($\alpha<0.05$) between compared sample sets. Scale bars: 100 μm

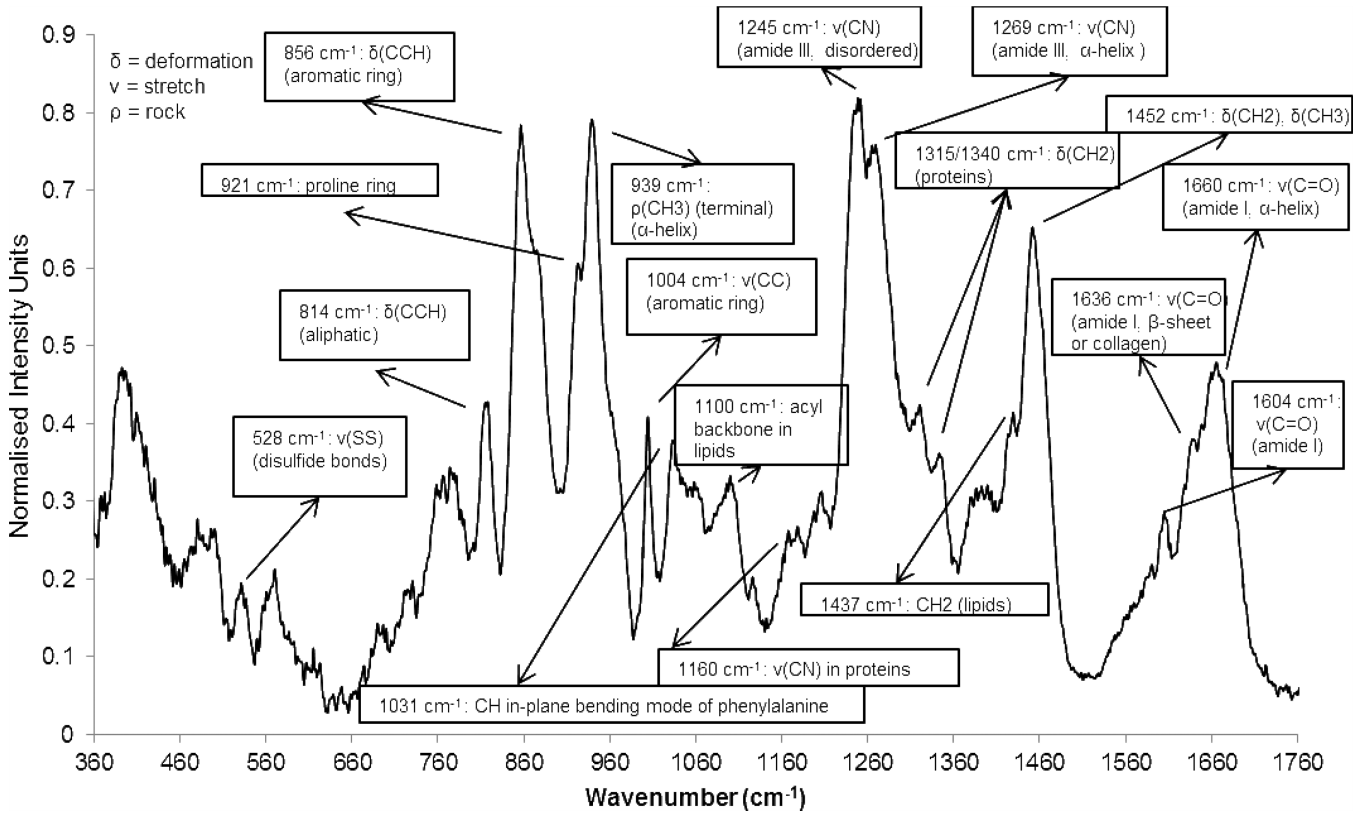

Figure 5.
Raman Spectra of porcine dermis with assignment of peaks.

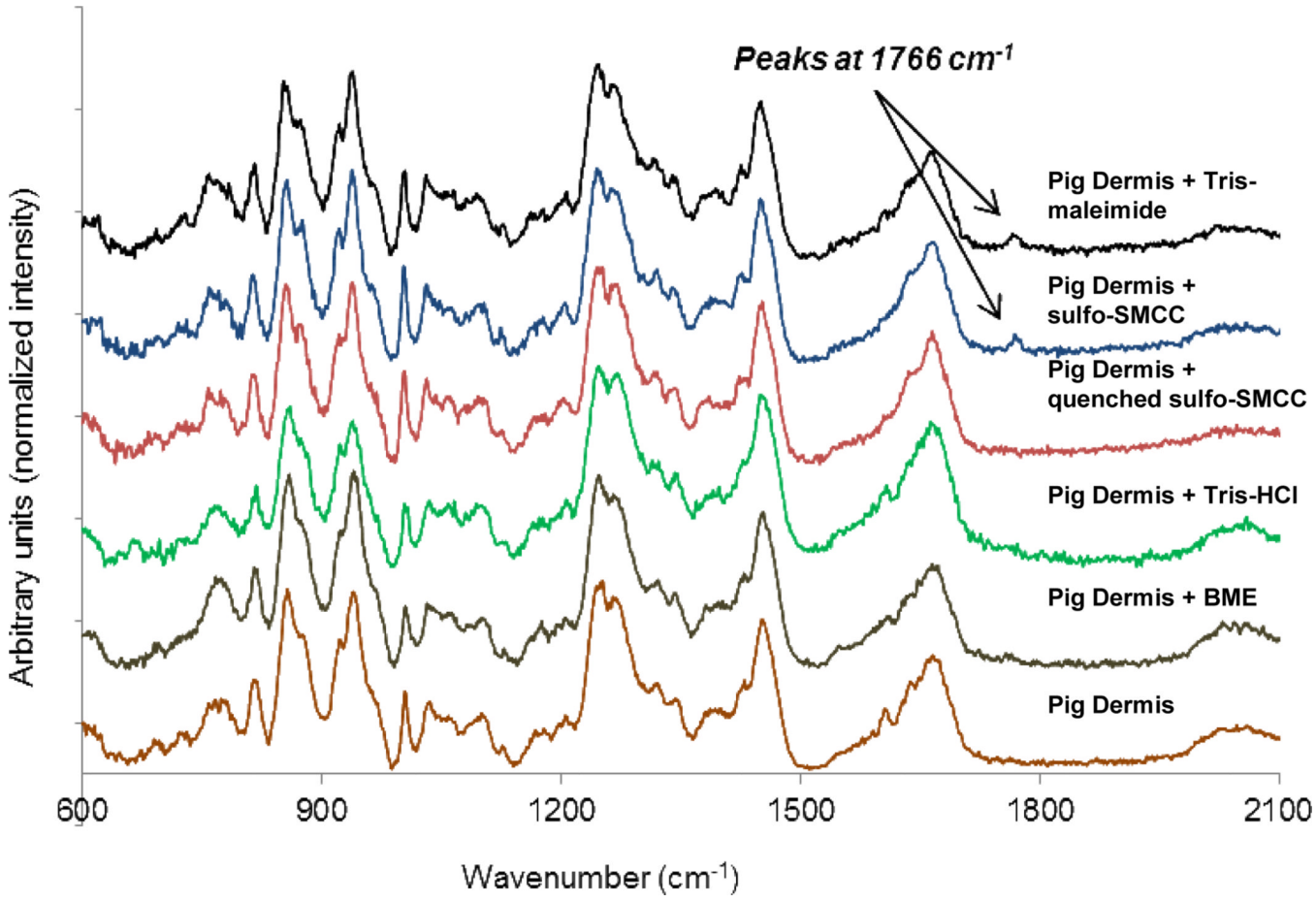

Figure 6.

Raman spectra of Pig Dermis Surface (PDS) treated with various chemical solutions for 1 hour followed by salt wash. Only the PDS treated with fresh, reactive hetero-bifunctional cross-linker (sulfo-SMCC) and partially quenched cross-linker (sulfo-SMCC whose amine-reactive end is quenched with Tris to give Tris-maleimide) show a peak at 1766 cm^{-1} (symmetric vibrational stretch for a cyclic imide group) indicating covalent attachment of maleimide group with sulfhydryl group on PDS.

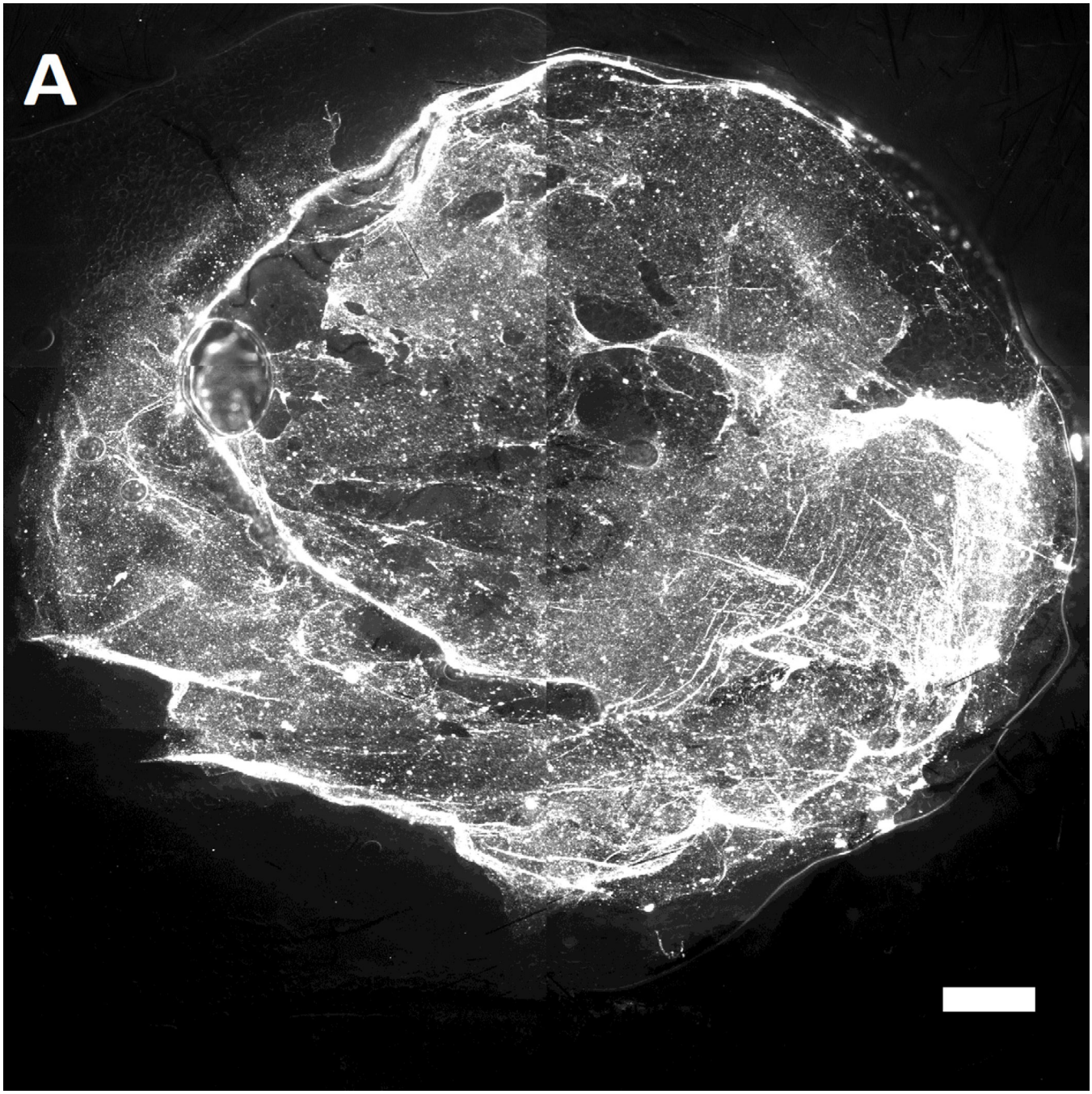

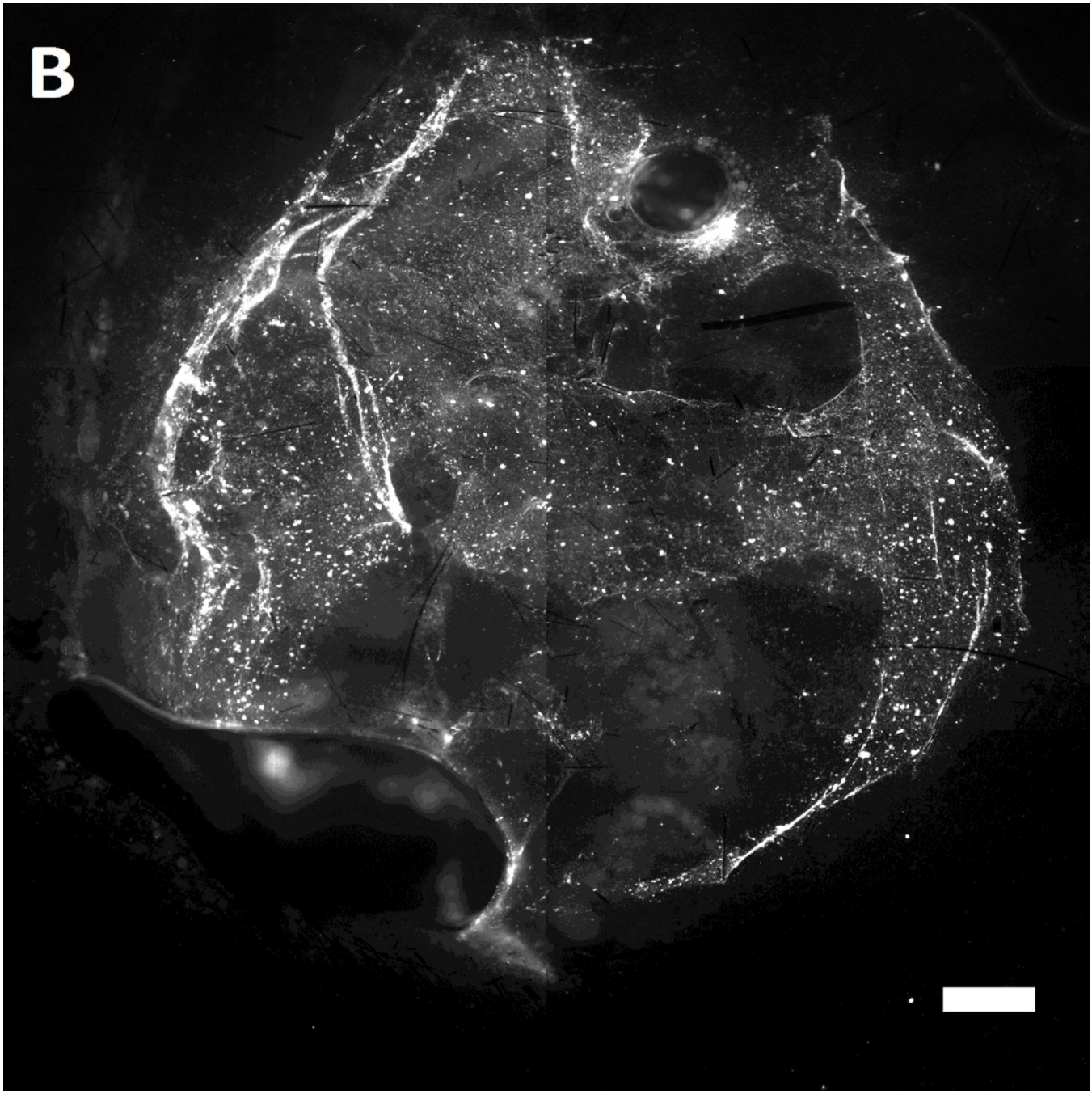

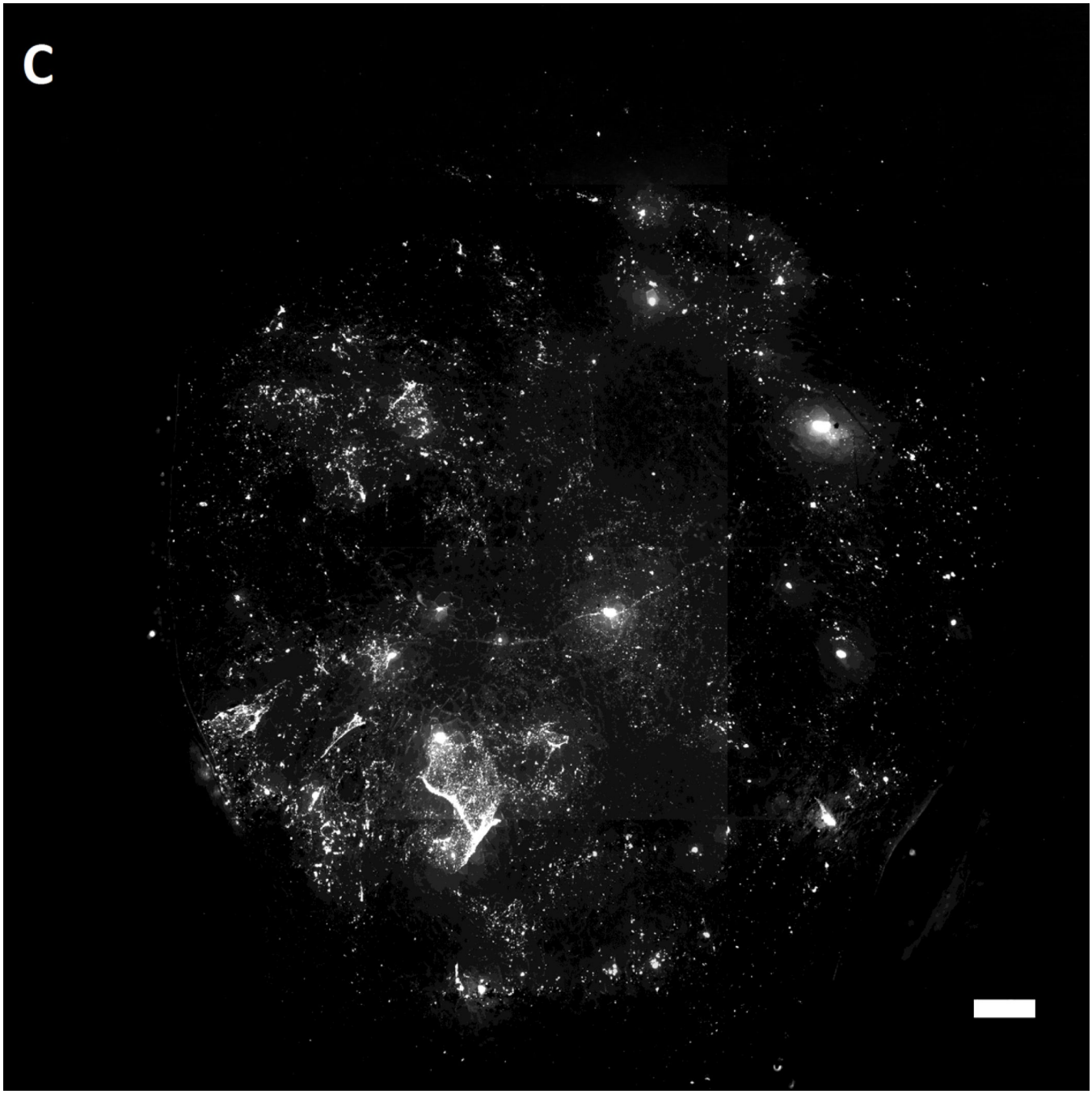

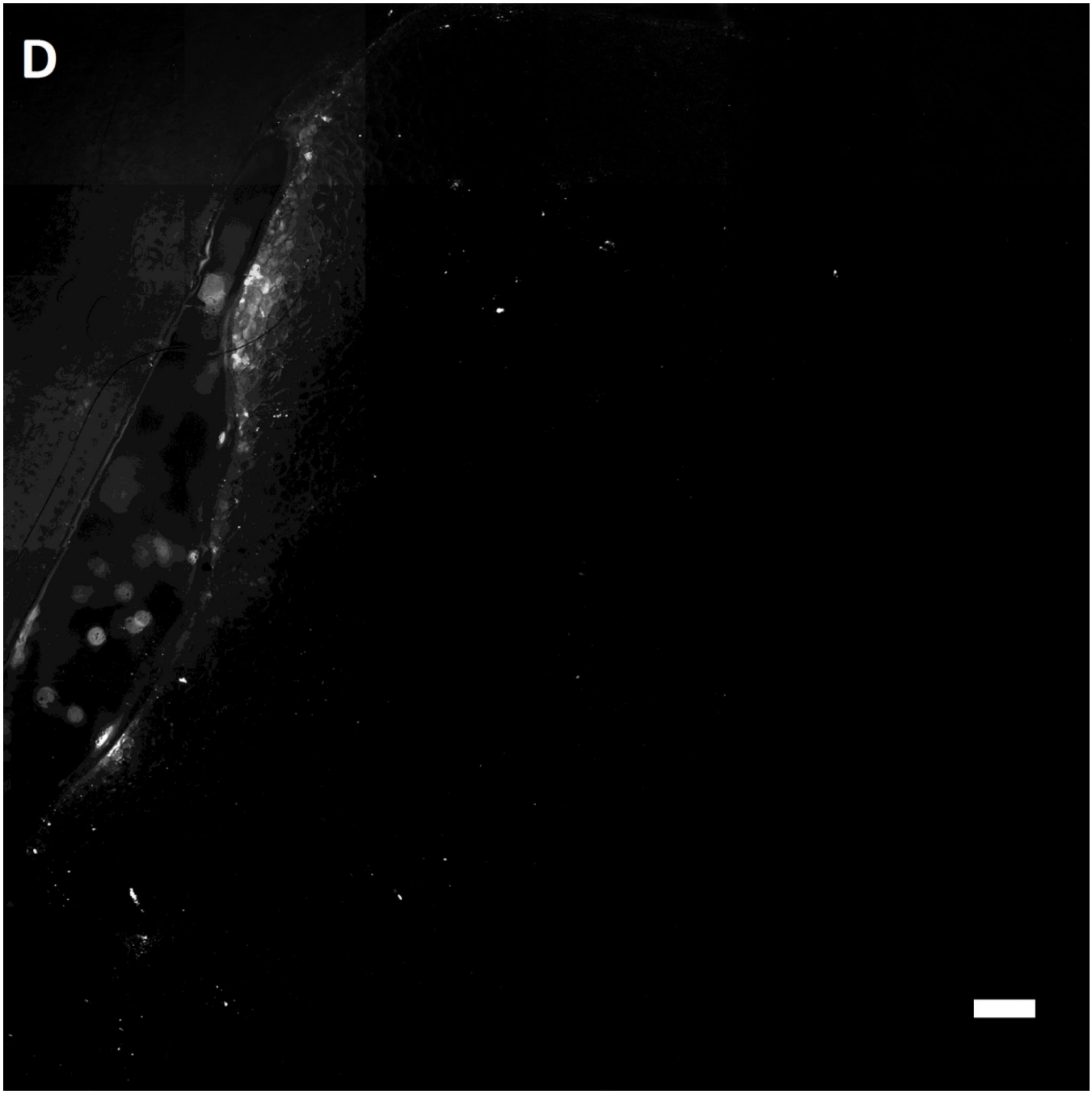

Figure 7.
Representative fluorescent images of live wild-type [A,B] and genetically diabetic [C,D] mice wounds (diameter: 4 mm.) treated with [A,C] sulfhydryl reactive microbeads (MAL-microbeads) and [B, D] non-reactive microbeads (NH_2-microbeads) for 30 mins followed by rinse with PBS (pH 7.4). Scale bars: 500 μm

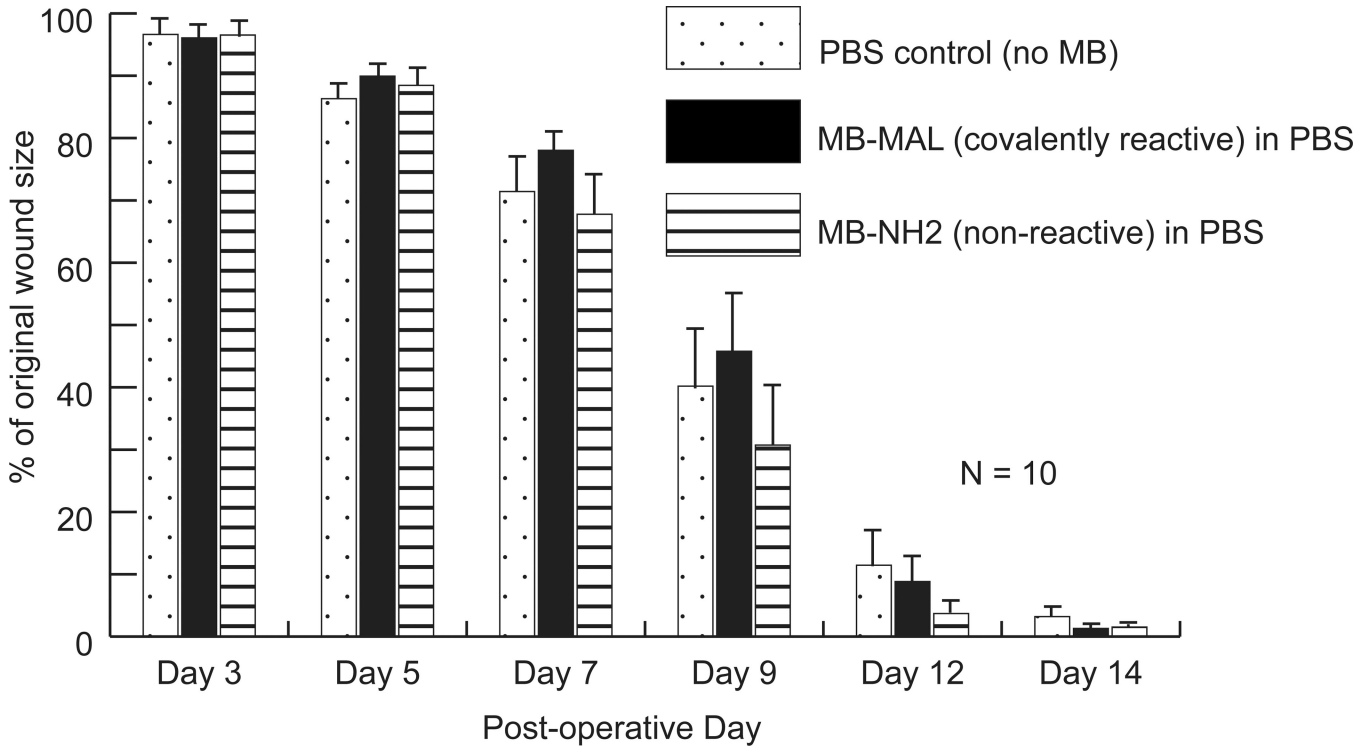

Figure 8.

Impairment of healing study on wild-type mice wounds. Three sets of mice (10 mice each) were treated with reactive MAL-microbeads suspended in PBS, non-reactive NH_2-microbeads suspended in PBS, and only PBS (no microbeads), respectively. Error-bars: +/− SEM.

Table 1

A summary of the chemical solutions that were incubated on porcine dermis samples for an hour in the Raman spectroscopic experiments.

Chemical solution in PBS (pH 7.4)	**Reactive Groups**	**Remarks**
Sulfo-SMCC only (6 mg/ml)	Maleimide and succinimide	Reactive towards –SH and –NH_2
Sulfo-SMCC (6 mg/ml) quenched with Tris-HCl (5× molar excess)	Maleimide	Reactive towards –SH only
Sulfo-SMCC (6 mg/ml) quenched with Tris-HCl (12 mg/ml, 5× molar excess) and 2-mercaptoethanol (6 mg/ml, 5× molar excess)	None	Fully quenched cross-linker solution
Tris-HCl only (12 mg/ml)	None	Control
2-mercaptoethanol (12 mg/ml)	None	Control
Blank control	None	Control